Article

Indirect Estimation of Tire Pressure on Several Road Pavements via Interacting Multiple Model Approach

Renato Brancati *,† and **Francesco Tufano** †

Department of Industrial Engineering, University of Naples Federico II, Corso Umberto I, 40, 80138 Naples, Italy
* Correspondence: renato.brancati@unina.it
† These authors contributed equally to this work.

Abstract: Generally, tire deflation results in a decrease in both handling performance and tire lifetime, and in fuel consumption increment. Therefore, the real-time knowledge of the pressure is important. Direct approaches via pressure sensors mounted on the rim of each tire are not practical, due to technical and economic reasons. Cost-effective solutions with real-time estimation of tire pressure are generally less accurate and reliable than direct ones. Dynamical estimators based on a suspension model need road surface topology information to compute disturbances on the suspension system as an input, which is typically unknown. This paper proposes an innovative approach to estimate tire pressure indirectly, without actual road surface roughness information. A vertical suspension dynamic model is used to build several unscented Kalman filters, parametrised around different road surface topologies. These estimators are combined following the Interacting Multiple Model approach, which gives an acceptable estimation of tire stiffness through a weighted average obtained from a probabilistic model. A known linear static relationship between the tire stiffness and inflation pressure is utilized to indirectly estimate the tire inflation pressure. A Monte Carlo analysis has been performed on a wide range of driving scenarios and vehicle manoeuvres. The results of the estimation have been compared to those of a single unscented Kalman filter, in order to validate the effectiveness of the proposed solution and to highlight the improved performances in monitoring tire pressure.

Keywords: indirect tire pressure monitoring system; unscented Kalman filter; interacting multiple model

1. Introduction

Tire pressure has a significant influence on the behaviour of vehicles, especially in terms of safety, consumption and wear. In 2007, the National Highway Traffic Safety Administration (NHTSA) in the USA had already published a legal regulation (FMVSS 138) requiring the installation of a tire pressure monitoring system (TPMS) in light vehicles. In 2012, the European Union also issued a similar regulation. Starting from 2014, the TPMS is mandatory in USA and in some European countries. An underinflated tire induces: a reduction of tire-road interaction forces; an undesirable steering behaviour; an increase of fuel consumption; or an unexpected blowout due to high temperature. An overinflated tire induces an undesirable steering behaviour and an uneven wear. The NHTSA estimates that about 55% of vehicles have at least one underinflated tire causing the waste of 2.8 billion gallons of fuel and about 260,000 accidents per year. Moreover, a low inflating pressure in tires reduces tire tread life by 15% and increases the frequency of tire changes [1]. When the tire inflation pressure measurement is realized by means of sensors mounted on the rim of tires, the TPMS is classified as "direct" (dTPMS). In addition to the sensors in a direct TPMS, there are devices for signal transmission and processing. The direct-type TPMS is characterized by high precision, but it has high costs. Each sensor is equipped with a battery that has to be replaced or recharged periodically. Winter tires also need their own

sensors. Therefore, a puncture or replacement requires an additional activity for the tire dealer and additional costs.

As an alternative to dTPMS, techniques that allow the estimation of the inflation pressure in the absence of pressure sensors have been developed. By exploiting the measurements of the sensors already present in the vehicle, this type of TPMS is classified as "indirect" (iTPMS). As early as 1996, an inflation tire pressure indirect measurement technique was proposed by Mayer [2]. Some methods based on measurement of angular velocity or wheel vertical acceleration are also described by Isermann in "Automotive control: modelling and control of vehicles" [3].

By comparing the four angular speeds, Personn [4] identifies the wheel that loses pressure.

Due to the roughness of the road and the torsional deformation of the tire, an oscillation of the angular velocity is induced. Tire stiffness is affected by inflation pressure so, as the pressure value changes, so does the wheel speed oscillation frequency.

Some iTPMS using different angular speed frequency analysis techniques have been proposed [4].

The algorithms use [5] the wheel vertical acceleration frequency analysis to estimate the inflation pressure.

The algorithms exploiting the measurement of both angular velocity and vertical acceleration are very interesting too [6].

Another class of estimation algorithms use the vehicle dynamics. In particular, Solmaz [7] starts from the measurements of lateral acceleration, yaw rate, steering angle and vehicle speed available by ESC system to estimate lateral vehicle dynamics state, together with the detection of tire pressure drops.

Reina [8] also starts from the ESP measurements, but he exploits the vehicle vertical dynamics to build the prediction model of a Kalman filter estimator for tire stiffness.

Road roughness is a critical unknown input for the model-based estimator [9], but often it is overlooked in the previously proposed estimation techniques.

Recently, Lee [10] addressed this problem and proposed an iTPMS based on Adaptive Extended Kalman Filter (AEKF) that can estimate both the pressure and the roughness of the road. However, since the vertical vehicle dynamics is characterized by great complexity and can further vary unexpectedly with the road roughness, an estimator based on a single dynamical model can exhibit poor closed-loop performances. As a result, it may be subject to significant estimation errors.

In this paper, a novel estimation algorithm based on vehicle vertical dynamics is proposed. In particular, the Unscented Kalman Filter (UKF) technique is considered to indirectly estimate the tire inflation pressure. To take into account the unknown road surface profile, an innovative procedure was ad hoc developed.

Specifically, an Interactive Multiple Model (IMM) estimator was considered to deal with abrupt changes of road roughness. This algorithm is composed of a bank of UKFs, each of them tailored to predict vertical dynamics behaviour when the vehicle is on a specific road with a specific degree of roughness. It can choose the model that best approximates the real dynamic behaviour for each instant. Many versions of IMM exist in the literature, based on the linear Kalman Filter (KF) or on its nonlinear version, such as the the Extended Kalman Filter (EKF) [11], the Unscented Filter [12,13]. The developed IMM combines four vertical vehicle dynamic models parameterized for four different road pavement types. Each filter gives a proper estimation of the vehicle state and covariance. All these estimations are combined through a weighted average obtained from a probabilistic model. Therefore, the IMM obtains the tire pressure estimation without an a-priori knowledge of the road surface. The method was validated by means of the dSPACE ASM vehicle dynamics simulation code [14].

Compared to the dPTMS, the proposed system has the advantage of having the accelerometers on the vehicle. This is the reason why they do not need to be replaced together with the tires, they can be easily powered, and they do not require a wireless data transmission to communicate the measurements.

2. Vehicle Dynamics and Road Profile Synthesis Modelling

The inflation pressure of the tire was estimated based on a two Degree-Of-Freedom (2DOF) Quarter Car (QC) non-linear model for passive suspensions, widely used to study, in ride comfort analyses, the vertical motion of vehicles caused by roads' surface unevenness [15]. It assumes the coupling of pitch, roll and heave motions of the vehicle are negligible, since it has poor significance for typical passenger-cars [16]. The model, in Figure 1, consists of basic elements of the suspension system such as sprung mass m_s (representing sprung mass of a vehicle quarter) connected via a spring and a damper (representing the suspension system) to the unsprung mass m_{us} (representing the wheel assembly).
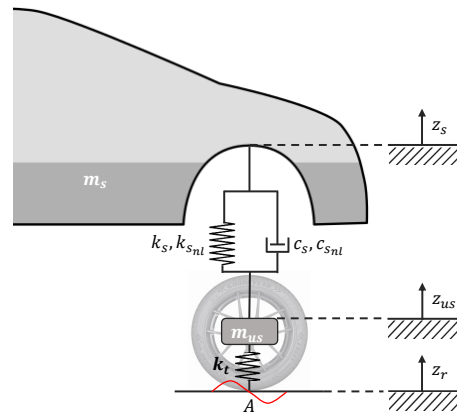

Figure 1. Quarter car model.

The fundamental assumption of the model is to neglect the effects of suspension systems' complex linkages [17]. Suspension systems generally exhibit non-linear behaviour [18], which can be taken into account considering a cubic stiffness $k_{s_{nl}}$ in parallel with a linear stiffness k_s [19], and a quadratic damping non-linearity modelled with linear c_s and non-linear damping coefficients $c_{s_{nl}}$ [15]. The vertical behaviour of the unsprung mass is modelled with a "single point contact model" approach [20], composed of a spring with a linear stiffness k_t (representing tire), while damping contribution is neglected [21]. It considers that the entire part of the tire in contact with the road is reduced to a single point contact A, which receives from the road a displacement according to its surface profile $z_r(t)$. This approach for modelling vehicle dynamics reduces the complexity of the system, while being highly effective [22]. For a 2DOF QC non-linear model representing 1/4th of a vehicle passive suspension system, according to d'Alembert's principle, the governing equations of motion are:

$$
\begin{aligned}
m_s\ddot{z}_s &= -k_s(z_s - z_{us}) - k_{s_{nl}}(z_s - z_{us})^3 - c_s(\dot{z}_s - \dot{z}_{us}) - c_{s_{nl}}(\dot{z}_s - \dot{z}_{us})^2 \\
m_{us}\ddot{z}_{us} &= -k_s(z_{us} - z_s) - k_{s_{nl}}(z_{us} - z_s)^3 - c_s(\dot{z}_{us} - \dot{z}_s) - c_{s_{nl}}(\dot{z}_{us} - \dot{z}_s)^2 - k_t(z_{us} - z_r)
\end{aligned}
\tag{1}
$$

with the sprung mass of a vehicle quarter m_s, calculated as [21]:

$$
m_s = \frac{1}{2}m_{s,vehicle}\frac{a_2}{l}
\tag{2}
$$

where, z_s is the vertical displacement of the sprung mass, z_{us} the is the vertical displacement (hop) of the unsprung mass, a_2 is the longitudinal distance of the centre of mass from the opposite axle, and l is the wheelbase. The total sprung mass of the vehicle $m_{s,vehicle}$ is calculated as the sum of vehicle chassis mass $m_{chassis}$ (vehicle body) and loading mass m_{load}, $m_{s,vehicle} = m_{chassis} + m_{load}$.

The proposed methodology indirectly estimates the tire pressure using its explicit relationship with the tire vertical stiffness. According to preliminary investigations, drawing an indirect estimation of tire inflation pressure by direct estimation of tire stiffness, during vehicle driving, seems to be a promising solution [8]. The relationship between the rolling dynamic vertical stiffness and the inflation pressure can be reasonably assumed

as linear [23], neglecting viscoelastic properties of the tire, since the 2DOF QC non-linear model operates under transient inputs [24]. This assumption can be successfully used to indirectly monitor the tire inflation pressure [10]. A linear relationship between vertical stiffness and inflation pressure of the tire is used [25]:

$$k_t = k_{t_0}\left(1 + p_{Fz_1} dpi\right) \tag{3}$$

with,

$$dp_i = \frac{p_{eff} - p_0}{p_0} \tag{4}$$

where, p_0 is the nominal pressure of the inflated tire, p_{eff} is the effective inflation pressure of the tire, k_{t_0} is the vertical stiffness at the nominal inflation pressure p_0, and p_{Fz_1} is the coefficient representing the pressure effect on vertical stiffness.

2.1. Road Surface Profile Synthesis

The 2DOF QC non-linear model reliable simulates vertical dynamics of vehicles if its input, road surface profile, is known. In this paper, we have adopted a methodology to synthesize the road profile numerically. Considering a single specific degree of road roughness, according to one of A–H classes of ISO (International Organization for Standardization) 8608 classification [26], the Power Spectral Density (PSD) of the road-velocity profile $\dot{z}_r$ can be assumed to be essentially flat [27]. Therefore, road input excitation, expressed as a velocity $\dot{z}_r$, can be represented as a white-noise. The road profile displacement z_r can be generated in time domain, non-linear vehicle models requirement, filtering the white-noise with a first-order linear shape filter [28]. We employ a method that provides for low frequency cutoff [29], with PSD $G_d(\omega)$ given by [30]:

$$G_d(\omega) = \frac{2\alpha v \sigma^2}{\pi} \frac{1}{(\alpha v)^2 + \omega^2} \tag{5}$$

where, ω is the angular frequency, σ^2 is the variance of road roughness, v is the vehicle longitudinal velocity, and α is the parameters that limit the maximum spectral height at low frequency. The road profile z_r, which has PSD given by (5), can be generated by the linear shape filter expressed as:

$$\frac{d}{dt}z_r(t) = -\alpha v z_r(t) + \eta(t) \tag{6}$$

where, $\eta(t)$ is a zero-mean Gaussian noise with a one-side PSD equal to $2\pi\alpha v\sigma^2$ [30], with the variance $\sigma^2 = 4G_d(\Omega_0)$ [31], considering the values of PSD at $\Omega_0 = 1$ rad/m as:

$$G_d(\Omega_0) = 4^a \times 10^{-6} \tag{7}$$

where, $a \in \{0, 1, \ldots, 7\}$, according to ISO 8608 [26]. From previous literature [31], the value of parameter α is set to 0.127 rad/m. Considering a lower spatial frequency limit $\Omega_L = 0.01$ cycles/m and an upper spatial frequency limit $\Omega_U = 10$ cycles/m the required length of generated road should be $L \geq 1/\Omega_L = 100$ m, while the sampling time $\Delta t \leq 1/(2\Omega_U v)$ [32]. This is a suitable methodology for the generation of a road surface profile, whose compatibility with ISO 8608 standard was assessed by Lee, D. H. et al. [33].

3. Interacting Multiple Model Filter

The road surface profile acts as a disturbance input to the suspension system, which is a critical issue in simulating car ride dynamics, since it is not known a-priori. The prediction model adopted partially mitigates this problem, generating an artificial profile of the road numerically, with the approach described in Section 2.1, used to compute road excitation

for the 2DOF QC model. However, reliable simulation of the effective car ride dynamics can be only carried out if the artificial road profile truly reflects the actual conditions.

The implemented methodology numerically generates road profiles conforming to a specific ISO class, according to the parameter a of the Equation (7). The road class that the vehicle is driving in is not known $a - priori$, and can abruptly change during driving. We address this issue through a Multiple Model (MM) approach; the MM system is governed by two relationships:

$$
\begin{aligned}
x_{\tau+1} &= f_s(x_\tau, u_\tau) + q \\
y_\tau &= h_s(x_\tau) + r
\end{aligned}
\tag{8}
$$

where $f_s(\cdot)$ is the process function, $h_s(\cdot)$ is the measurement function, $s \in \{0, 1, \ldots, S\}$ is the state mode , $x \in R^{n_x}$ is the state vector, and $y \in R^{n_y}$ is the measurement vector. The process q and measurement r noises are both assumed as zero-mean uncorrelated processes with covariances Q and R, respectively. The IMM system is composed of a bank of multiple KFs, identified by value of s, each of them tailored to represent ride dynamics behaviour of the vehicle for one of road classes that the vehicle could driving in. Here, nonlinear f_s and h_s are considered; thus nonlinear filters, such as UKFs, must be used. The interacting multiple model unscented filter (IMMUF) for estimation of tire inflation pressure is given by an algorithm composed of the following steps; for time step $\tau = 1, \ldots, \tau_f$:

1. Mode Probability Prediction:

$$
\hat{\mu}^{\tau|\tau-1} = Pz\hat{\mu}^{\tau-1|\tau-1}.
\tag{9}
$$

2. Mixing of the previous estimates:

$$
\hat{x}_{\tau-1|\tau-1}^{i,*} = \sum_{j=1}^{S} \frac{Pz_{i,j}\hat{\mu}_j^{\tau|\tau-1}\hat{x}_{\tau-1|\tau-1}^j}{\hat{\mu}_i^{\tau|\tau-1}},
\tag{10}
$$

$$
\hat{P}_{\tau-1|\tau-1}^{xx,i,*} = \sum_{j=1}^{S} \frac{Pz_{i,j}\hat{\mu}_j^{\tau|\tau-1}\hat{P}_{\tau-1|\tau-1}^{xx,j}}{\hat{p}_i^{\tau|\tau-1}}.
\tag{11}
$$

3. Mode dependent UKFs, whose equations can be found in [34].
4. Mode Probability Correction:

$$
\hat{\mu}_j^{\tau|\tau} = \frac{\hat{\mu}_j^{\tau|\tau-1}\exp\left(-\frac{1}{2}\left(v_\tau^j\right)^T\left(\hat{P}_{\tau|\tau-1}^{yy,j}\right)^{-1}v_\tau^j\right)}{c\det\left(\hat{P}_{\tau|\tau-1}^{yy,j}\right)},
\tag{12}
$$

5. IMMUF's corrected estimates:

$$
\hat{x}_{\tau|\tau} = \sum_{j=1}^{S}\hat{\mu}_j^{\tau|\tau}\hat{x}_{\tau|\tau}^j,
\tag{13}
$$

$$
\hat{P}_{\tau|\tau}^{xx} = \sum_{j=1}^{S}\hat{\mu}_j^{\tau|\tau}\left(\hat{P}_{\tau|\tau}^{xx,j} + \left(\hat{x}_{\tau|\tau}^j - \hat{x}_{\tau|\tau}\right)(\diamond)^T\right).
\tag{14}
$$

where, $\mu(s)$ is the probability vector, Pz is the Markov Transition Matrix (MTM) , P is the covariance matrix, v is a noise, c is a normalizing constant. Note that, considering a generic matrix A, $(A)(\diamond)$ stands for $(A)(A)$, and $\det(A)$ for the determinant of A.

4. Tire Inflation Pressure Estimation

The proposed IMMUF for estimation of the tire inflation pressure is schematized in Figure 2. It consists of a bank of UKF, each of them with a prediction model able to represent ride dynamics behaviour of the vehicle when driving on a road belonging to a specific ISO class. Usually, road profiles hardly belong to classes worse than D (repair

interventions should be performed to restore optimal conditions), so, only the classes A (very good), B (good), C (average) and D (poor) are considered; therefore, the proposed multiple model, to be able to estimate the inflation pressure when vehicle driving on roads whose roughness level can significantly change, a bank of four UKF is considered. The state vector considered is $x = [z_s, z_{us}, \dot{z}_s, \dot{z}_{us}, k_t]^T \in \mathbb{R}^{5 \times 1}$. Since measurements available to the IMMUF are the sprung and unsprung vertical acceleration, $\ddot{z}_s$ and $\ddot{z}_{us}$, the measurement vector is $y = [\ddot{z}_s, \ddot{z}_{us}]^T \in \mathbb{R}^{2 \times 1}$. To indirectly estimate the tire inflation pressure, the tire vertical stiffness k_t is modelled as a random walk process [35] that artificially varies the parameters at every sampling instant. Discretizing 2DOF QC nonlinear model equations through the forward Euler method, the particular nonlinear function $f_s(.)$ of the state equations is given by:

$$
\begin{cases}
z_{s_{\tau+1}} = z_{s_\tau} + [\dot{z}_{s_\tau}]\Delta t \\
z_{us_{\tau+1}} = z_{us_\tau} + [\dot{z}_{us_\tau}]\Delta t \\
\dot{z}_{s_{\tau+1}} = \dot{z}_{s_\tau} + \left[\dfrac{-k_s(z_{s_\tau}-z_{us_\tau}) - k_{s_{nl}}(z_{s_\tau}-z_{us_\tau})^3 - c_s(\dot{z}_{s_\tau}-\dot{z}_{us_\tau}) - c_{s_{nl}}(\dot{z}_{s_\tau}-\dot{z}_{us_\tau})^2}{m_s} \right]\Delta t \\
\dot{z}_{us_{\tau+1}} = \dot{z}_{us_\tau} + \left[\dfrac{-k_s(z_{us_\tau}-z_{s_\tau}) - k_{s_{nl}}(z_{us_\tau}-z_{s_\tau})^3 - c_s(\dot{z}_{us_\tau}-\dot{z}_{s_\tau}) - c_{s_{nl}}(\dot{z}_{us_\tau}-\dot{z}_{s_\tau})^2 - k_{t_\tau}(z_{us_\tau}-z_r)}{m_{us}} \right]\Delta t \\
k_{t_{\tau+1}} = k_{t_\tau} + w_{t_\tau}
\end{cases}
\tag{15}
$$

where, w_{t_τ} is assumed to be zero mean Gaussian white noise process with variance σ_t. The measurement function $h_s(.)$ is as follows:

$$
\begin{cases}
\ddot{z}_{s_\tau} = \dfrac{-k_s(z_{s_\tau}-z_{us_\tau}) - k_{s_{nl}}(z_{s_\tau}-z_{us_\tau})^3 - c_s(\dot{z}_{s_\tau}-\dot{z}_{us_\tau}) - c_{s_{nl}}(\dot{z}_{s_\tau}-\dot{z}_{us_\tau})^2}{m_s} \\
\ddot{z}_{us_\tau} = \dfrac{-k_s(z_{us_\tau}-z_{s_\tau}) - k_{s_{nl}}(z_{us_\tau}-z_{s_\tau})^3 - c_s(\dot{z}_{us_\tau}-\dot{z}_{s_\tau}) - c_{s_{nl}}(\dot{z}_{us_\tau}-\dot{z}_{s_\tau})^2 - k_{t_\tau}(z_{us_\tau}-z_r)}{m_{us}}
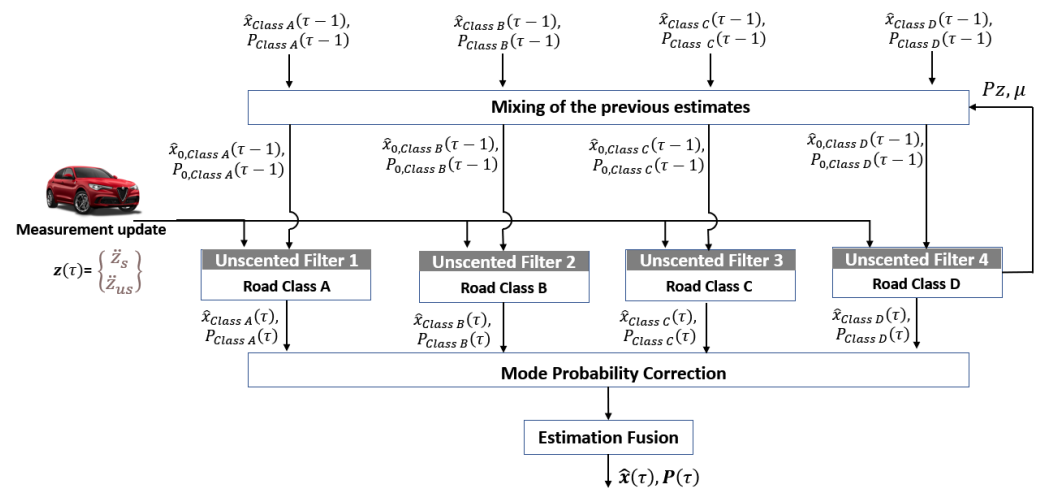\end{cases}
\tag{16}
$$

Figure 2. Scheme of the interacting multiple model unscented filter.

The MTM Pz, to assign the same probability to each mode, is defined as:

$$
Pz = \begin{pmatrix}
0.97 & 0.01 & 0.01 & 0.01 \\
0.01 & 0.97 & 0.01 & 0.01 \\
0.01 & 0.01 & 0.97 & 0.01 \\
0.01 & 0.01 & 0.01 & 0.97
\end{pmatrix}
\tag{17}
$$

The process noise covariance matrix Q is defined as:

$$Q = \begin{pmatrix} q_1\Delta t^3 & 0 & 0 & 0 & 0 \\ 0 & q_2\Delta t^3 & 0 & 0 & 0 \\ 0 & 0 & q_3\Delta t^3 & 0 & 0 \\ 0 & 0 & 0 & q_4\Delta t^3 & 0 \\ 0 & 0 & 0 & 0 & q_5\Delta t^3 \end{pmatrix} \tag{18}$$

where q_0–q_5 are five tuning parameters of the IMMUF, and Δt is the sampling time of the filter. While the covariance matrix of measurement noise R_ν is defined as:

$$R_\nu = \begin{pmatrix} \sigma_{az_s} & 0 \\ 0 & \sigma_{az_{us}} \end{pmatrix} \tag{19}$$
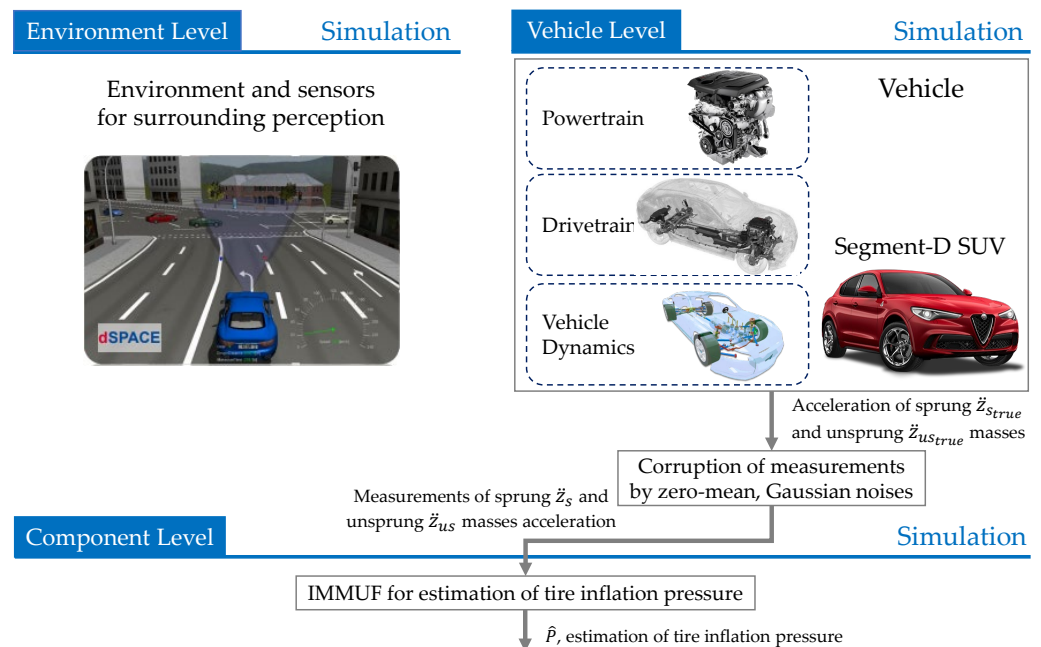
being σ_{az_s} and $\sigma_{az_{us}}$ the respective standard deviations.

5. Algorithm Validation

In this section, the effectiveness of the approach is assessed through a numerical campaign. First Monte Carlo simulation was carried out to compare tire inflation pressure estimation accuracy by the proposed methodology with respect to a single unscented filter. Then, the capability of the IMMUF to deal with abruptly change of road surface profile class and tire inflation pressure was verified.

5.1. Simulation Platform

High-fidelity simulations were executed to assess the accuracy of tire inflation pressure estimation. The simulation platform used consists of a three-levels architecture, in Figure 3.
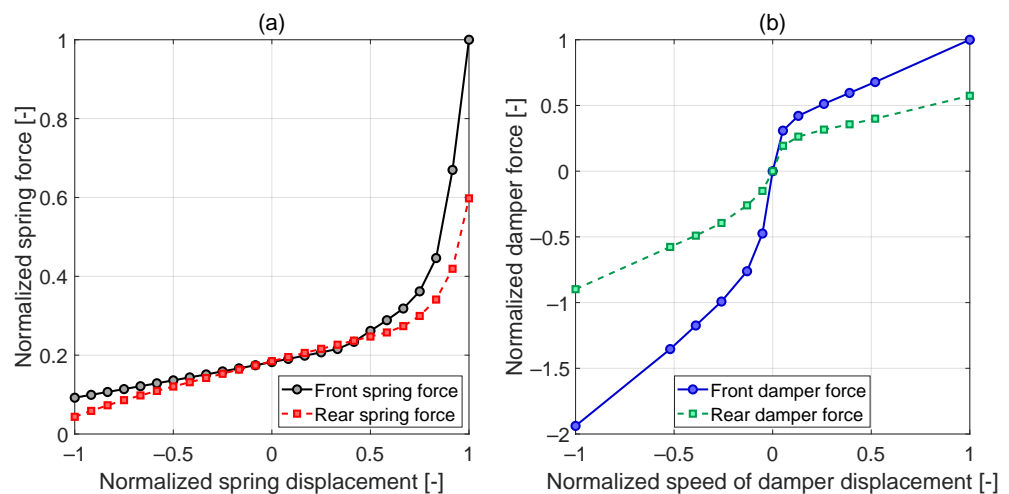

Figure 3. High-fidelity vehicle simulation environment.

The first layer is composed of models for simulation of the environment and sensors for the surrounding perception. The second layer consists of models for the simulation of a Segment-D SUV vehicle, whose parameters are reported in Table 1 [36]. Then, in the third layer, the algorithm for the estimation of tire inflation pressure.

Table 1. Segment-D SUV vehicle parameters.

Quantity	Value	Quantity	Value
Mass of vehicle chassis $m_{chassis}$ (vehicle body)	1788 kg	Height of the center of mass h_g	0.6 m
Front semi-wheelbase a_1	1.347 m	Rear semi-wheelbase a_2	1.471 m
Front track width t_1	1.606 m	Rear track width t_2	1.6364 m
Yaw moment of inertia J_z	3230 kg m^2	Frontal area S_a	2.75 m^2
Front wheel mass $m_{us,F}$	61.14 kg	Rear wheel mass $m_{us,R}$	52.75 kg
Nominal pressure of inflated tire p_0	250 kPa	vertical stiffness k_{t_0} at p_0	264,700 N/m

Simulation of the Segment-D SUV vehicle was carried out with the dSPACE software Automotive Simulation Model (ASM). It allows us to model the longitudinal, lateral, and vertical dynamics of passengers' cars through a multi-body approach: the vehicle is composed of 5 bodies (15 degrees of freedom), the vehicle and four wheels (4 d.o.f. of the system represent the vertical speed of the wheels), including suspension kinematics and forces, tire-road contact forces and torques (TNO MF-Tyre 6.1), aerodynamics, steering, and brakes. In the vehicle simulation software, the suspension system is modelled in order to include nonlinearities in the analysis of the dynamic of the vehicle. The suspension system of the vehicle consists of double wishbones in the front axle, and a multi-link configuration in the rear axle. Figure 4 shows the spring and damper characteristics.

Figure 4. (**a**) Spring force. (**b**) Damper force.

5.2. 2DOF QC Parameters Identification

As mentioned above, the IMMUF consists of a bank of four UF, each with different parameterisations for the prediction model. Specifically, the approach provides one model properly parametrised to represent the ride dynamics behaviour of the vehicle for each of A - D road classes that the vehicle could driving in. Herein, for each of these four classes, we have tailored a prediction model to the ASM high-fidelity vehicle simulation by levering the results obtained from several numerical simulations [37]. By doing so, we have obtained prediction models that reliable reproduce the ride dynamics behaviour of the vehicle under several roads, belonging to A - D classes, such that they can be exploited for the estimation methodology. Four system identification problems have been solved, one for each of the A - D road classes, any of them formulated as an optimization task where the objective was to find a set of parameters that minimizes the prediction error between outputs of the ASM simulation, and the 2DOF QC model [38]. Two outputs have been considered, the vertical accelerations of sprung $\ddot{z}_s$ and unsprung $\ddot{z}_{us}$ masses, here computed considering the tire inflation pressure (parameter to be estimated) and the road surface profile (that acts as unknown input during estimation) as known inputs. More specifically, the outputs have been computed in nine simulation scenarios, by combining

three vehicle speeds (40, 60 and 80 km/h) and three tire inflation pressures (130, 180 and 230 kPa), in a straight-line manoeuvre, considering the road model of ASM environment subsystem set to provide properties of road according to one of the classes. The exploited identification procedure has been performed four times, changing the road from class A to D, which, leveraging a Genetic Algorithm (GA), found four sets of parameters for the 2DOF QC model, respectively. Each prediction model is characterized by 12 parameters, four of which, listed in the Table 2, were unknown and needed to be identified; therefore we have considered these four parameters as decision variables of the optimization task.

Table 2. 2DOF QC model unknown parameters.

Parameter	Description
c_s	Linear damping coefficient
$c_{s_{nl}}$	Non-linear square damping coefficient
k_s	Linear spring stiffness coefficient
$k_{s_{nl}}$	Non-linear cube spring stiffness coefficient

The Root Mean Square Error (RMSE) between the ASM simulation and the 2DOF QC model outputs, $\ddot{z}_s$ and $\ddot{z}_{us}$, in the nine simulation scenarios, have been defined as objective functions to be minimized, as:

$$\sqrt{\frac{1}{N} \sum_{k=1}^{N} (z_s(\tau) - \hat{z}_s(\tau))^2} \tag{20}$$

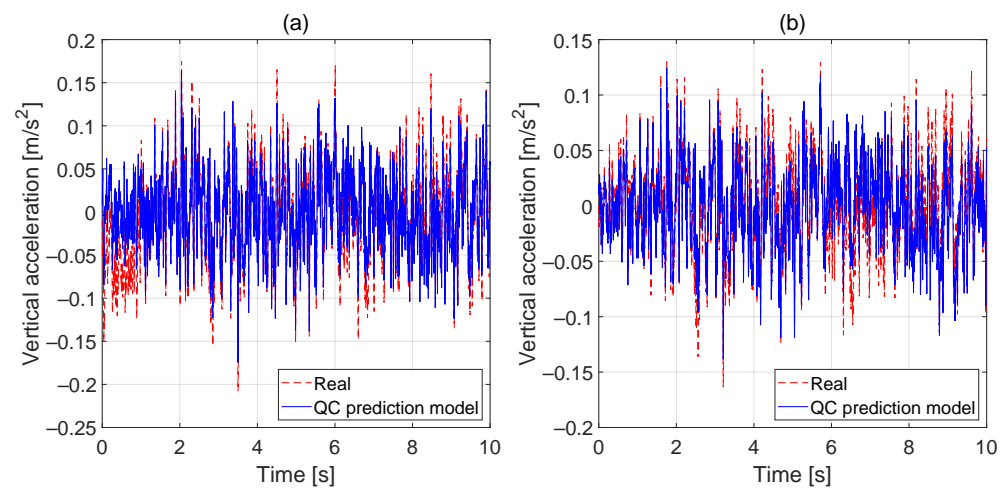$$\sqrt{\frac{1}{N} \sum_{k=1}^{N} (z_{us}(\tau) - \hat{z}_{us}(\tau))^2} \tag{21}$$

where, N is the number of samples.

The population size was set according to the technical literature [39], while, the one-point crossover method and the bit-string mutation were used for the crossover and the mutation, respectively [40]. The number of generation was set to 1000, enough for identifying solutions belonging to the 18-dimensional hypersurface of the Pareto frontier. Among the dominant solutions, the one situated at the minimum distance from the origin of the 18-dimensional hyperspace was considered. Solutions of the four system identification problems are reported in Table 3, where each of its columns contains parameter values for the 2DOF QC model exploitable to simulate ride dynamics behaviour of the vehicle under test on roads belonging to one of the four A - D classes.

Table 3. Optimal solutions of the four system identification problems.

Parameter	Road Class A	Road Class B	Road Class C	Road Class D
c_s [Ns/m]	6576	4585	14,819	14,708
$c_{s_{nl}}$ [Ns/m^2]	4319	6016	5839	4555
k_s [N/m]	113,086	173,415	94,544	118,114
$k_{s_{nl}}$ [N/m^3]	130,098	151,886	62,836	121,723

The results of the identification problems, therefore, have a poor physical meaning, since they not are the real stiffness and damping coefficients of the vehicle suspension system, but are values identified by the optimization methodology to reproduce the input/output behaviour of the vehicle system, as shown by Figure 5.

Figure 5. Unsprung mass acceleration; (**a**) tire inflation pressure 230 kPa; and (**b**) tire inflation pressure 130 kPa. Vehicle speed 60 km/h, road class B.

5.3. Monte Carlo Simulation

To assess the tire inflation pressure estimation accuracy by the proposed methodology, a Monte Carlo numerical campaign has been carried out. The Monte Carlo method is generally used to evaluate the uncertainty of estimations [41], since it leads to more advantages then conventional methods, which require the evaluation of the separate effect of each input quantity on the result through a parametric analysis [42]. When, in a complex system, multiple input variables are correlated, uncertainty analysis become a not trivial task and sometimes even unreliable. Monte Carlo simulation [43,44] is a probabilistic method to solve deterministic problems thanks to the use of electronic calculators, which can simulate a lot of experimental trials that have random outcomes. When applied to uncertainty evaluation, random numbers are generated to randomly sample parameters' uncertainty space. Such an analysis is closer with the probabilistic nature of the actual processes.

Both the IMMUF and the single UF solutions have been tested executing a set of 100 simulations, where the initial conditions have been varied according to $\hat{x}_{0|0} \in \mathcal{N}(x_0, \sqrt{P_{0|0}})$, with $P_{0|0} = diag[\sigma^2_{z,s}, \quad \sigma^2_{z,us}, \quad \sigma^2_{v_z,s}, \quad \sigma^2_{v_z,us}, \quad \sigma^2_{k,t}]$.

Straight-line manoeuvres were executed in all Monte Carlo simulations, varying the tire inflation pressure p_{eff}, ISO class of road profile according to the parameter a of the Equation (7), and the vehicle speed v, according to a uniform distribution in the ranges of Table 4.

Table 4. Scenario parameters range.

Parameter	Range
p_{eff}	(130–230) [kPa]
v	40–80 [km/h]
a	0–3 [-]

The measurements employed in the IMMUF are acquired with the high-fidelity vehicle simulation model and corrupted by zero-mean, Gaussian noises:

$$\begin{cases} \ddot{z}_s = \ddot{z}_{s_{true}} + \nu_{az_s}, & \nu_{az_s} \in \mathcal{N}(0, \sigma_{az_s}) \\ \ddot{z}_{us} = \ddot{z}_{us_{true}} + \nu_{az_{us}}, & \nu_{az_{us}} \in \mathcal{N}(0, \sigma_{az_{us}}) \end{cases} \quad (22)$$

where, σ_{az_s} and $\sigma_{az_{us}}$ are the values of the noise covariances. In this numerical campaign, they were both set equal to 0.5 m/s^2, as reported in the sensors datasheets. The single UF used to compare the results is based on the same model parametrised for the road class A. The results of the Monte Carlo simulation require a post-processing to clearly represent the uncertainty of the estimation algorithm. Four indexes have been considered:

- Mean estimation error from all the Monte Carlo samples $\in \{1, \ldots, j, \ldots, N\}$ (the red line in Figure 6). For each τ-th time step, the mean estimation error is calculated as

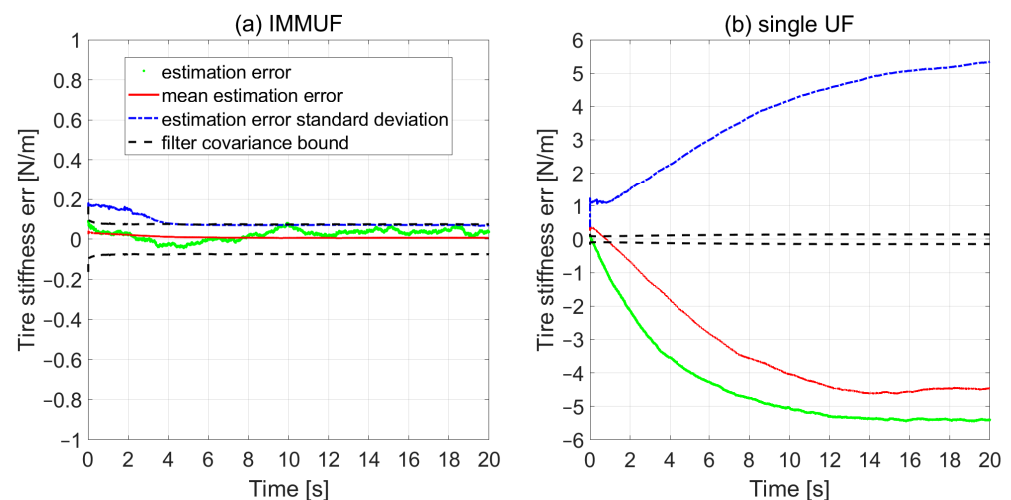$$\overline{Err_\tau} = \frac{\sum_{j=1}^{N} k_{t_{\tau,j}} - \hat{k}_{t_{\tau,j}}}{N} \quad (23)$$

- Standard deviation of the estimation errors (the dashed blue line in Figure 6). For each τ-th time step, the standard deviation of the errors is calculated as

$$\sqrt{\frac{1}{N-1} \sum_{j=1}^{N} |Err_{\tau,j} - \overline{Err_\tau}|^2} \quad (24)$$

- Covariance bound σ computed by the filter (the dashed black line in Figure 6). For each τ-th time step, the σ-bounds is calculated by the square root of the diagonal elements of the covariance matrix P, as

$$\frac{\sum_{j=1}^{N} \sqrt{P_{\tau,j}}}{N} \quad (25)$$

- Comparison of sample estimation error (the green line in Figure 6) with the σ-bounds.

Figure 6. (**a**) IMMUF and (**b**) classic UF estimation error on k_t.

The results show how the IMMUF outperforms the single filter solution: the mean error is around zero; the standard deviation converges to the same values of the σ-bounds, lower than the single UF solution; and the sample estimation error remains within the σ-bounds for all the simulation time. These results confirm the possibility to use a Multiple Model algorithm to deal with more realistic and non-trivial scenarios.

5.4. Tire Inflation Pressure Estimation

To assess the capability of IMMUF to deal with abrupt changes of road surface profile class and tire inflation pressure, several numerical simulations have been executed. Figure 7 shows the results of a simulation scenario where a road profile according to ISO class A was considered. In the top, it can be noted that after 2 of 10 s of simulation, the IMMUF converges to an acceptable estimation of tire inflation pressure. In the bottom of Figure 7 are reported the moving average of each single mode estimation: as shown, mode 1, exploitable for estimation on roads of class A, fast converges to a real value of tire inflation pressure, while the other modes diverge to much lower values. Similarly, Figure 8 shows the results of a simulation executed on a road with a ISO class D profile, confirming the capability of the IMMUF to estimate tire inflation pressure on different road, without a-priori information on surface profile.
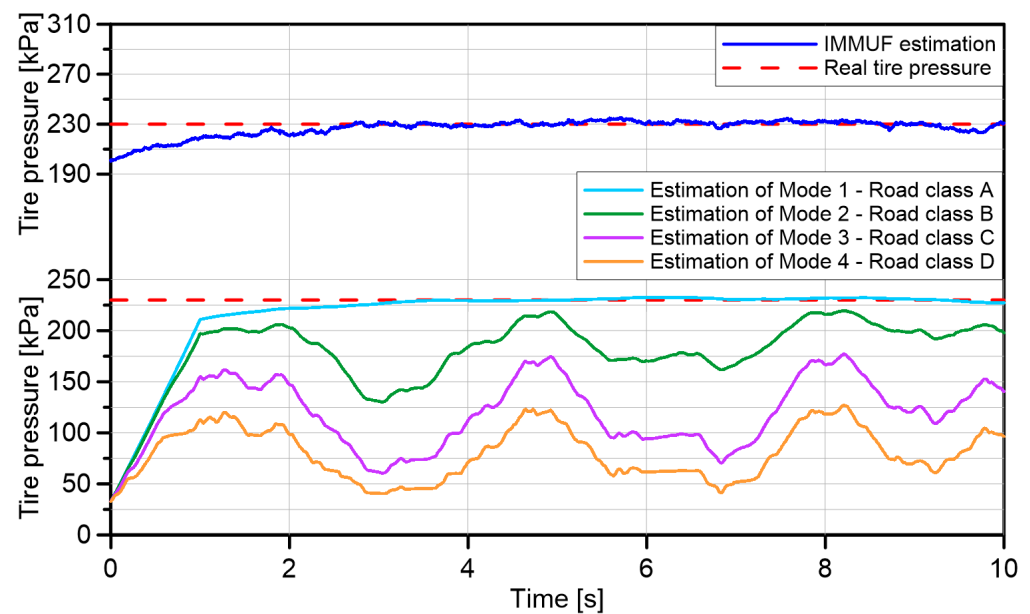
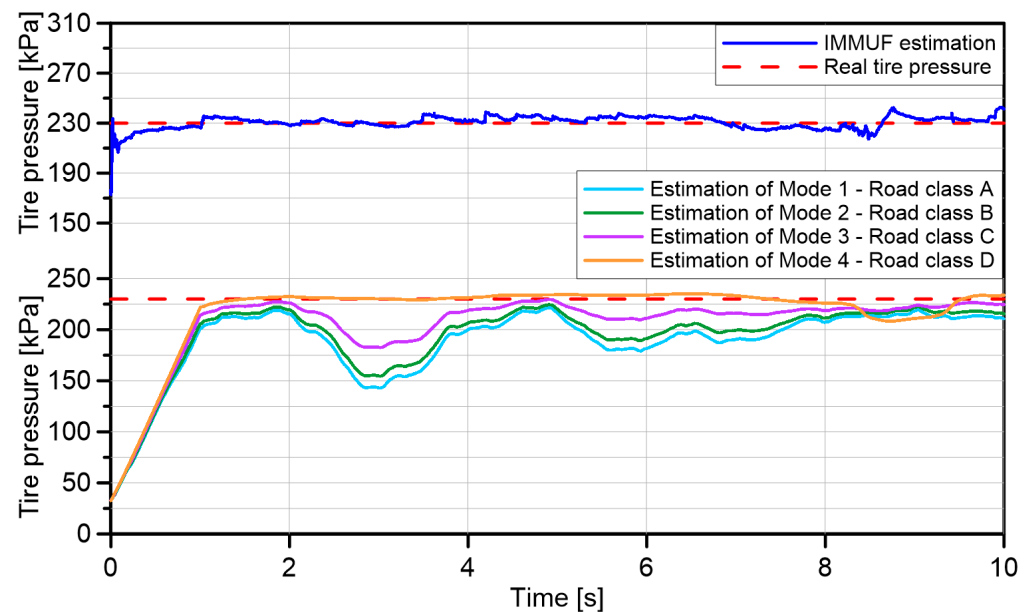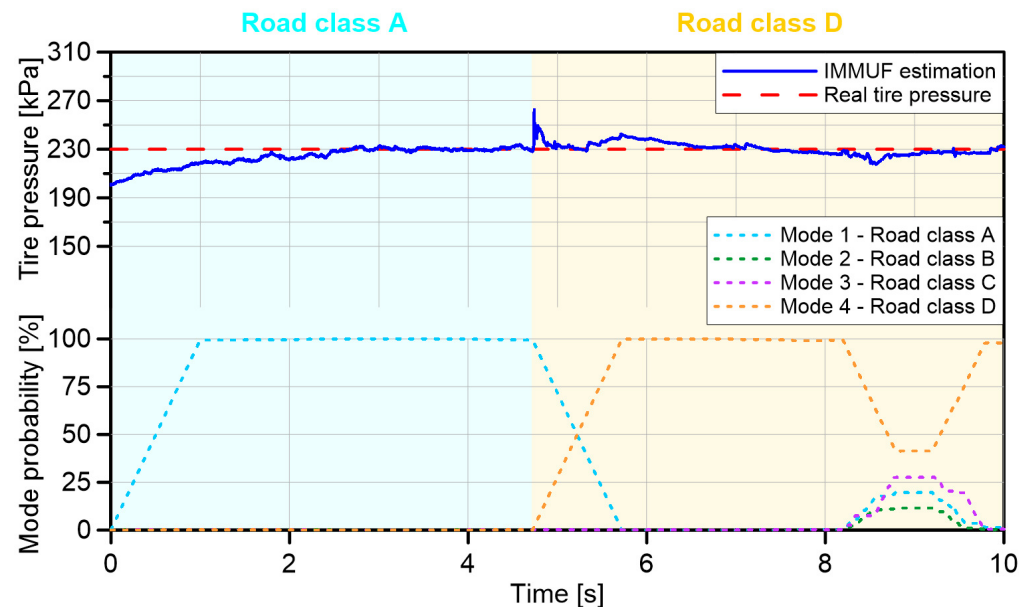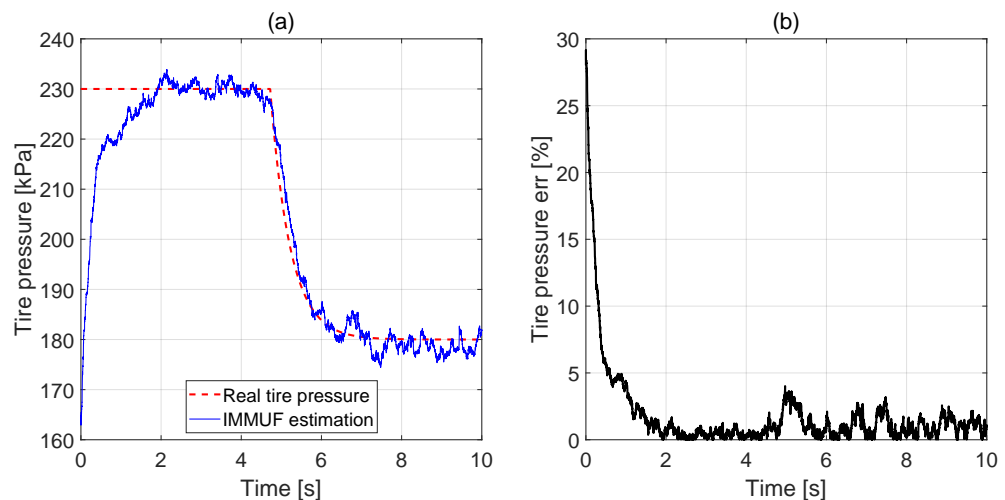**Figure 7.** Estimation of tire pressure on an ISO class A road.

Figure 8. Estimation of tire pressure on an ISO class D road.

To verify the capability of the IMMUF to deal with abrupt changes of road surface profile class, a scenario with two different road surface profiles has been considered. For 5 s of simulation, the vehicle drives on a class A road, and then, with a sudden change of road profile, drives on a class D road. The results, shown in Figure 9, highlight how the MM approach is able to deal with changes of road pavement conditions, as usually happens in real-world driving. Comparing the measurements to every single prediction, claims are made as to which filter most likely represents the true vehicle dynamics. According to it, the algorithm steps provide for evaluation of the likelihood function of each filter, and their probability is so updated, in order to place more trust in that filter. In particular, for the first 5 s of simulation (class A road), mode 1 has been the most representative, while in the last 5 s (class D road), more trust has been placed in mode 4, as highlighted by the moving averages of modes probability showed in the bottom of Figure 9. Instead, to verify the capability of the IMMUF to estimate tire deflection, a simulation on a class B road was executed, with a sudden reduction of tire inflation pressure from 230 kPa to 180 kPa in

about 1.5 s (Figure 10). The estimation converges to a real tire inflation pressure value in about 2 s, and then accurately follows the transient behaviour without significant delay in response to the pressure drop, with a low estimation error.

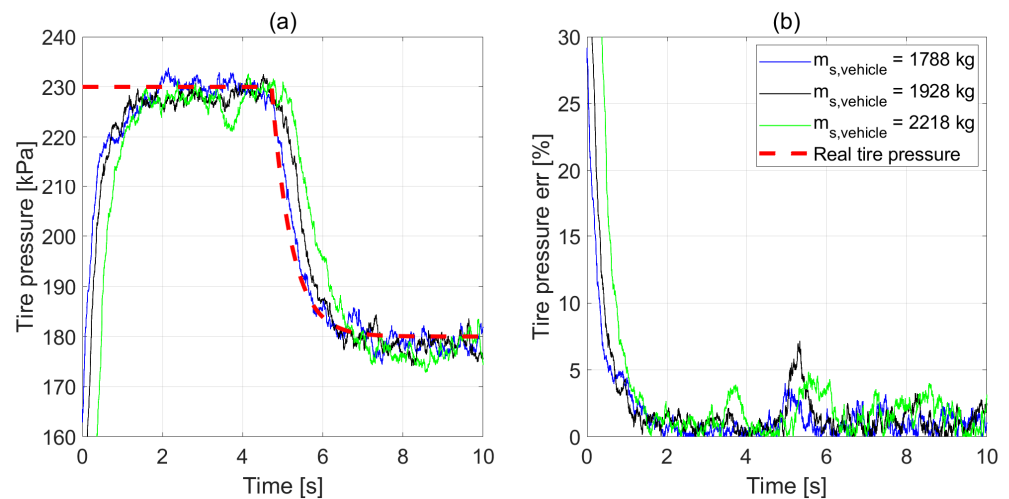**Figure 9.** Estimation of tire pressure with abrupt change of class for road surface profile.

Figure 10. (**a**) Estimation of tire pressure with abrupt change of tire inflation pressure and (**b**) estimation error.
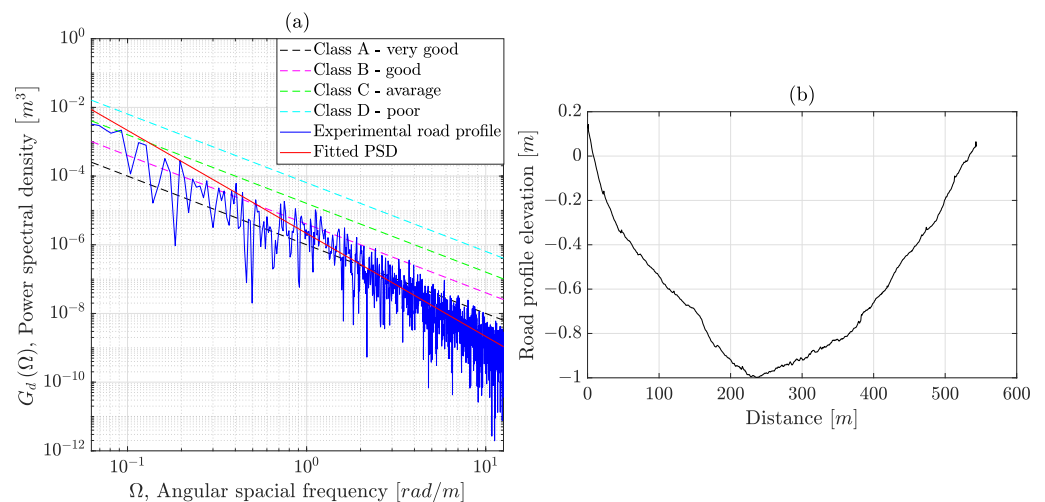
A sensitivity analysis has been carried out to investigate the reliability of the proposed algorithm with respect to the variability of the sprung mass of the vehicle, because the vehicle sprung mass depends on loading, which is one of the significant model uncertainties leading to mismatched process noise. Considered constant, the sprung mass of the quarter car model, the nominal sprung mass of the vehicle in the high-fidelity simulation (empty vehicle, 1788 kg) was perturbed by +8% (1928 kg) and +24% (2218 kg), respectively, as shown in Figure 11. The estimated and actual inflation pressure show good agreement in the three scenarios. The results highlight the reliability of the estimation algorithm against the uncertainty on vehicle unsprung mass because the mean estimation error is lower than 5%. This behaviour confirms the well-known robustness of the Kalman filter against mismatched process noise covariance due to parameter uncertainty [45].

Finally, capability of the proposed algorithm to accurately estimate the tire inflation pressure without information on road surface roughness, on any type of road pavement

whose surface roughness belongs to $A - D$ ISO 8608 classification, was proven. To this purpose, an experimental measure of road roughness measured with a mobile LIDAR system, and reported in [46], has been used. In Figure 12 is plotted the road displacement Power Spectral Density (PSD) versus angular spatial frequency in a bi-logarithmic plan. In particular, a simulation scenario was considered, that consists of the Segment-D SUV vehicle driving in a road, whose roughness profile is reproduced according to the road roughness measure. Simulation results, in Figure 13, show how the algorithm successfully estimates the tire inflation pressure, confirming, in a real-word scenario, the capability of the multiple model approach to work on any type of road pavement, dealing with unknown road surface roughness.
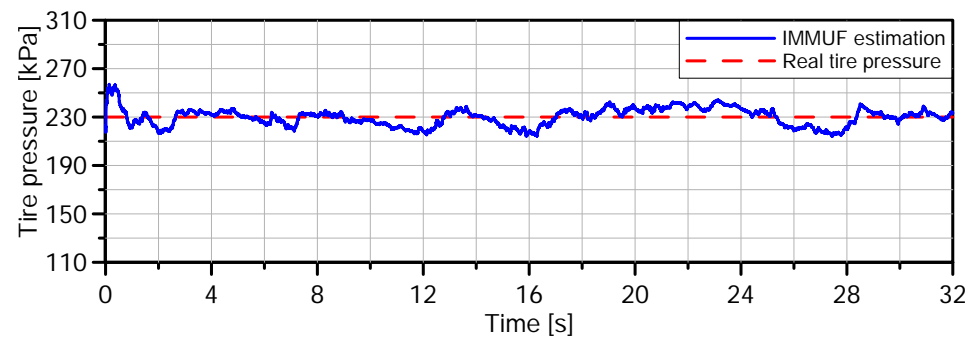

Figure 11. (**a**) Estimation of tire pressure with respect to different total sprung mass of the vehicle $m_{s,vehicle}$ and (**b**) estimation errors.

Figure 12. (**a**) Power spectral density of (**b**) experimental road profile.

Figure 13. Estimation of tire pressure with experimental road.

6. Conclusions

In this paper, an innovative algorithm for the estimation of tire inflation pressure was presented. The estimation is based on an Interacting Multiple Model Unscented Filter scheme that considers a bank of four UF, each of them exploitable for estimation of ride dynamics behaviour of a car on different road surface profiles, belonging to A - D ISO classes. The validation of the algorithm was carried out with an extensive numerical campaign, using a simulation platform representative of a real SUV vehicle, developed with dSPACE software ASM. Numerical simulations have confirmed the validity of the approach and have disclosed how the estimation of tire inflation pressure could be successfully carried to detect tire deflation, also when the road profile changes. The next steps will concern the evaluation of real time applicability, and definition of the procedure for on-board measured data input selection, which define the limits for vehicle manoeuvres exploitable for estimation purposes.

Author Contributions: Conceptualization, R.B. and F.T.; methodology, F.T.; software, F.T.; validation, R.B. and F.T.; formal analysis, R.B. and F.T.; investigation, F.T.; writing—original draft preparation, R.B. and F.T.; writing—review and editing, R.B. and F.T.; supervision, R.B. and F.T. All authors have read and agreed to the published version of the manuscript.

Institutional Review Board Statement: Not applicable.

Informed Consent Statement: Not applicable.

Data Availability Statement: Not applicable.

Conflicts of Interest: The authors declare no conflict of interest.

Abbreviations

The following abbreviations are used in this manuscript:

NHTSA	National Highway Traffic Safety Administration
TPMS	Tire Pressure Monitoring System
dTPMS	direct Tire Pressure Monitoring System
iTPMS	indirect Tire Pressure Monitoring System
KF	Kalman Filter
EKF	Extended Kalman Filter
UKF	Unscented Kalman Filter
MM	Multiple Model
IMM	Interactive Multiple Model
IMMUF	Interacting Multiple Model Unscented Filter
2DOF	Two Degree Of Freedom

QC	Quarter Car
PSD	Power Spectral Density
MTM	Markov Transition Matrix
RMSE	root Mean Square Error
ASM	Automotive Simulation Model

Nomenclature

The following symbols are used in this manuscript:

Symbol	Description	Symbol	Description
m_s	Sprung mass	m_{us}	Unsprung mass
$m_{chassis}$	vehicle chassis mass	m_{load}	loading mass
$m_{s,vehicle}$	total sprung mass of the vehicle	l	wheelbase
a_2	rear semiwheel base	dp_i	inflation pressure increment
c_s	Linear damping coefficient	$c_{s_{nl}}$	Non-linear square damping coefficient
k_s	Linear spring stiffness coefficient	$k_{s_{nl}}$	Non-linear cube spring stiffness coefficient
k_t	Tire stiffness coefficient	k_{t0}	vertical stiffness at the nominal inflation pressure
z_s	sprung mass vertical displacement	z_{us}	unsprung mass vertical displacement

Symbol	Description	Symbol	Description
z_r	road profile	p_0	nominal pressure
p_{eff}	effective pressure	p_{Fz1}	pressure effect on vertical stiffness
ω	angular frequency	$G_d(\omega)$	PSD
σ^2	road roughness variance	v	vehicle longitudinal velocity
α	linear shape filter parameter	$\mu(t)$	probability vector
Ω_0	reference spacial frequency	Ω_L	lower spatial frequency
Ω_U	upper spatial frequency	Pz	Probability transition matrix
Q	process noise covariance matrix	$x(t)$	state vector
$y(t)$	measurement vector	f_s	process function
h_s	measurement function	P	covariance matrix
R_v	noise covariance matrix	σ^2_{azs}	sprung mass acceleration variance
τ	time step	v	noise

References

1. Elfasakhany, A. Tire Pressure Checking Framework: A Review Study. *Reliab. Eng. Resil.* **2019**, *1*, 12–28.
2. Mayer, A.; Emig, G.; Gmehling, B.; Popovska, N.; Hölemann, K.; Buck, A. Passive regeneration of catalyst coated Knitted fiber Diesel particulate traps. *SAE Trans.* **1996**, *105*, 36–44.
3. Isermann, R. *Automotive Control: Modeling and Control of Vehicles*; Springer: Berlin/Heidelberg, Germany, 2022.
4. Persson, N.; Gustafsson, F.; Drevö, M. Indirect tire pressure monitoring using sensor fusion. *SAE Trans.* **2002**, *111*, 1657–1662.
5. Weispfenning, T. Fault detection and diagnosis of components of the vehicle vertical dynamics. *Meccanica* **1997**, *32*, 459–472. [CrossRef]
6. Isermann, R.; Wesemeier, D. Indirect vehicle tire pressure monitoring with wheel and suspension sensors. *IFAC Proc. Vol.* **2009**, *42*, 917–922. [CrossRef]
7. Solmaz, S. A Novel Method for Indirect Estimation of Tire Pressure. *J. Dyn. Syst. Meas. Control* **2016**, *138*, 054501. [CrossRef]
8. Reina, G.; Gentile, A.; Messina, A. Tyre pressure monitoring using a dynamical model-based estimator. *Veh. Syst. Dyn.* **2015**, *53*, 568–586. [CrossRef]
9. Kang, S.W.; Kim, J.S.; Kim, G.W. Road roughness estimation based on discrete Kalman filter with unknown input. *Veh. Syst. Dyn.* **2019**, *57*, 1530–1544. [CrossRef]
10. Lee, D.H.; Yoon, D.S.; Kim, G.W. New indirect tire pressure monitoring system enabled by adaptive extended Kalman filtering of vehicle suspension systems. *Electronics* **2021**, *10*, 1359. [CrossRef]
11. Tsunashima, H.; Murakami, M.; Miyataa, J. Vehicle and road state estimation using interacting multiple model approach. *Veh. Syst. Dyn.* **2006**, *44*, 750–758. [CrossRef]
12. Battistini, S.; Brancati, R.; Lui, D.G.; Tufano, F. Enhancing ADS and ADAS Under Critical Road Conditions Through Vehicle Sideslip Angle Estimation via Unscented Kalman Filter-Based Interacting Multiple Model Approach. In *Proceedings of the Advances in Italian Mechanism Science*; Springer International Publishing: Cham, Switzerland, 2022; pp. 450–460.
13. Ping, X.; Cheng, S.; Yue, W.; Du, Y.; Wang, X.; Li, L. Adaptive estimations of tyre–road friction coefficient and body's sideslip angle based on strong tracking and interactive multiple model theories. *Proc. Inst. Mech. Eng. Part D J. Autom. Eng.* **2020**, *234*, 3224–3238. [CrossRef]
14. Musa, A.; Pipicelli, M.; Spano, M.; Tufano, F.; De Nola, F.; Di Blasio, G.; Gimelli, A.; Misul, D.A.; Toscano, G. A review of model predictive controls applied to advanced driver-assistance systems. *Energies* **2021**, *14*, 7974. [CrossRef]

15. Mohite, A.G.; Mitra, A.C. Development of linear and non-linear vehicle suspension model. *Mater. Today Proc.* **2018**, *5*, 4317–4326. [CrossRef]
16. Sayers, M.W. *The Little Book of Profiling: Basic Information about Measuring and Interpreting Road Profiles*; Technical Report; University of Michigan, Transportation Research Institute: Ann Arbor, MI, USA, 1998.
17. Hurel, J.; Mandow, A.; García-Cerezo, A. Kinematic and dynamic analysis of the McPherson suspension with a planar quarter-car model. *Veh. Syst. Dyn.* **2013**, *51*, 1422–1437. [CrossRef]
18. McGee, C.G.; Haroon, M.; Adams, D.E.; Luk, Y.W. A frequency domain technique for characterizing nonlinearities in a tire-vehicle suspension system. *J. Vib. Acoust.* **2005**, *127*, 61–76. [CrossRef]
19. Nagarkar, M.P.; Patil, G.J.V.; Patil, R.N.Z. Optimization of nonlinear quarter car suspension–seat–driver model. *J. Adv. Res.* **2016**, *7*, 991–1007. [CrossRef]
20. Lemaitre, J. *Handbook of Materials Behavior Models, Three-Volume Set: Nonlinear Models and Properties*; Elsevier: Amsterdam, The Netherlands, 2001.
21. Guiggiani, M. *The Science of Vehicle Dynamics*; Springer: Pisa, Italy, 2014; p. 15.
22. Maher, D.; Young, P. An insight into linear quarter car model accuracy. *Veh. Syst. Dyn.* **2011**, *49*, 463–480. [CrossRef]
23. Wong, J.Y. *Theory of Ground Vehicles*; John Wiley & Sons: Hoboken, NJ, USA, 2022.
24. Taylor, R.; Bashford, L.; Schrock, M. Methods for measuring vertical tire stiffness. *Trans. ASAE* **2000**, *43*, 1415–1419. [CrossRef]
25. Besselink, I.; Schmeitz, A.; Pacejka, H. An improved Magic Formula/Swift tyre model that can handle inflation pressure changes. *Veh. Syst. Dyn.* **2010**, *48*, 337–352. [CrossRef]
26. *ISO (International Organization for Standardization) 8608:2016*; Mechanical Vibration—Road Surface PROFILES—Reporting of Measured Data. Available online: https://www.iso.org/standard/71202.html (accessed on 18 October 2022).
27. Ulsoy, A.G.; Peng, H.; Çakmakci, M. *Automotive Control Systems*; Cambridge University Press: Cambridge, UK, 2012.
28. Tyan, F.; Hong, Y.F.; Tu, S.H.; Jeng, W.S.; Generation of random road profiles. *J. Adv. Eng.* **2009**, *4*, 1373–1378.
29. Dharankar, C.S.; Hada, M.K.; Chandel, S. Numerical generation of road profile through spectral description for simulation of vehicle suspension. *J. Braz. Soc. Mech. Sci. Eng.* **2017**, *39*, 1957–1967. [CrossRef]
30. Schiehlen, W. White noise excitation of road vehicle structures. *Sadhana* **2006**, *31*, 487–503. [CrossRef]
31. Goenaga, B.; Fuentes, L.; Mora, O. Evaluation of the methodologies used to generate random pavement profiles based on the power spectral density: An approach based on the International Roughness Index. *Ing. E Investig.* **2017**, *37*, 49–57. [CrossRef]
32. Shannon, C.E. Communication in the presence of noise. *Proc. IRE* **1949**, *37*, 10–21. [CrossRef]
33. Lenkutis, T.; Čerškus, A.; Šešok, N.; Dzedzickis, A.; Bučinskas, V. Road surface profile synthesis: Assessment of suitability for simulation. *Symmetry* **2020**, *13*, 68. [CrossRef]
34. Battistini, S.; Menegaz, H.M. Interacting multiple model unscented filter for tracking a ballistic missile during its boost phase. In Proceedings of the 2017 IEEE Aerospace Conference, Big Sky, MT, USA, 4–11 March 2017; pp. 1–8.
35. Varshney, D.; Bhushan, M.; Patwardhan, S.C. State and parameter estimation using extended Kitanidis Kalman filter. *J. Process Control* **2019**, *76*, 98–111. [CrossRef]
36. Stellantis. Segment-D SUV Vehicle Specifications' Documents. 2022. Available online: https://stellantis-na-product-media.info/alfa-romeo/stelvio (accessed on 29 November 2022).
37. Maino, C.; Misul, D.; Musa, A.; Spessa, E. Optimal mesh discretization of the dynamic programming for hybrid electric vehicles. *Appl. Energy* **2021**, *292*, 116920. [CrossRef]
38. Gimelli, A.; Luongo, A.; Muccillo, M. Efficiency and cost optimization of a regenerative Organic Rankine Cycle power plant through the multi-objective approach. *Appl. Therm. Eng.* **2017**, *114*, 601–610. [CrossRef]
39. Brancati, R.; Muccillo, M.; Tufano, F. Crank mechanism friction modeling for control-oriented applications. In *Proceedings of the The International Conference of IFToMM ITALY*; Springer: Cham, Switzerland, 2020; pp. 729–737.
40. Petrillo, A.; Prati, M.V.; Santini, S.; Tufano, F. Improving the NOx reduction performance of an Euro VI d SCR System in real-world condition via nonlinear model predictive control. *Int. J. Engine Res.* 2021 . [CrossRef]
41. Papadopoulos, C.E.; Yeung, H. Uncertainty estimation and Monte Carlo simulation method. *Flow Meas. Instrum.* **2001**, *12*, 291–298. [CrossRef]
42. De Nola, F.; Giardiello, G.; Noviello, B.; Tufano, F. A control-oriented and physics-based model of the engine crank mechanism friction for the base calibration: Parametric analysis. In *Proceedings of the AIP Conference Proceedings*; AIP Publishing LLC: College Park, MD, USA, 2019; Volume 2191, p. 020060.
43. Harding, B.; Tremblay, C.; Cousineau, D. Standard errors: A review and evaluation of standard error estimators using Monte Carlo simulations. *Quant. Methods Psychol.* **2014**, *10*, 107–123. [CrossRef]
44. Harrison, R.L. Introduction to monte carlo simulation. In *Proceedings of the AIP Conference Proceedings*; American Institute of Physics: College Park, MD, USA, 2010; Volume 1204, pp. 17–21.
45. Ge, Q.; Shao, T.; Duan, Z.; Wen, C. Performance analysis of the Kalman filter with mismatched noise covariances. *IEEE Trans. Autom. Control* **2016**, *61*, 4014–4019. [CrossRef]
46. Šroubek, F.; Šorel, M.; Žák, J. Precise international roughness index calculation. *Int. J. Pavement Res. Technol.* **2022**, *15*, 1413–1419. [CrossRef]